Performance of BDS navigation ionospheric model during the main phase of different classified geomagnetic storms in China region

Junchen Xue [1], Marcio Aquino [2], Sreeja Vadakke Veettil[2], Xiaogong Hu [1], Lin Quan [3]

[1]Shanghai Astronomical Observatory, Chinese Academy of Sciences, Shanghai, China
[2]Nottingham Geospatial Institute, University of Nottingham, Nottingham, UK
[3]Beijing Institute of Tracking and Communication Technology, Beijing, China

Key Points:

- The influence on the accuracy of the model during strong storms is greatest, followed by moderate and weak storms.
- The impact on the accuracy of the model is clearly characterized by the latitude and local time.
- The accuracy of the model is not comparable for the same class of storms.

Corresponding author: Junchen Xue, jcxue@shao.ac.cn

This article has been accepted for publication and undergone full peer review but has not been through the copyediting, typesetting, pagination and proofreading process, which may lead to differences between this version and the Version of Record. Please cite this article as doi: 10.1029/2019RS007033

Abstract

Geomagnetic storms can have a great impact on the Earth's upper atmosphere, i.e. the ionosphere. The activity of the ionosphere could be more pronounced during geomagnetic storms, which can make key ionospheric parameters, like total electron content (TEC), very hard to be modelled. The use of a Global Navigation Satellite System (GNSS) navigation ionospheric model is a conventional option for users to correct the ionospheric delay, which could suffer from the effects of storms. In this study, the performance of Beidou Navigation Satellite System (BDS) navigation ionospheric model in the China region during the main phase of different classes of geomagnetic storms is investigated for the first time. The analysis of the results revealed that the accuracy of the BDS navigation ionospheric model was impacted to different degrees during the storms. The effects during strong storms were the greatest, followed by moderate and weak storms. The impact on the accuracy of the model was characterized by latitude and local time. Furthermore, the accuracy of the model during the same class of storms was not always at the same level. The finding in this study could benefit the prediction of GNSS navigation ionospheric models' performance during geomagnetic storms.

1 Introduction

Geomagnetic storms are magnetospheric disturbances which are characterized by increased particle fluxes in the ring current. The enhanced fluxes can be measured as a reduction in the horizontal component of the geomagnetic field (Echer et al., 2008). Geomagnetic storms are primarily motivated by intense, long duration and southward interplanetary magnetic fields (IMFs). The southward IMFs interconnect with the geomagnetic field and transport the solar wind energy into the Earth's magnetosphere (Gonzalez et al., 1999). A geomagnetic storm can be subdivided into three phases: initial, main and recovery. The main phase is the most influential part of a geomagnetic storm (Gonzalez et al., 1994; Loewe & Prölss, 1997).

Geomagnetic storms can induce the largest global atmospheric effects (Lastovicka, 1996). The ionosphere responds to geomagnetic storms with signs like depletion or enhancement of electron content. The response might be quite different during the storms, which depends on the location and local time of the geomagnetic storm onset (Danilov & Lastovicka, 2001). The ionosphere can be disturbed by geomagnetic storms from high latitudes (D'Angelo et al., 2018), middle latitudes (Amabayo et al., 2012; Heelis et al., 2009), to low latitudes (Chakraborty et al., 2015; Sreeja et al., 2009). The key parameters for the ionosphere, such as total electron content (TEC), height of F2 (hmF2) and frequency of F2 (foF2) could be affected to various grades (Blagoveshchenskii, 2013; Dujanga et al., 2013; Ngwira et al., 2012) during storms.

Radio signals can be reflected, refracted and diffracted when propagating in the ionosphere. During geomagnetic storms the ionospheric activity could be more complicated, which can impact radio propagation dependent applications. It is conventional to apply ionospheric models to correct the background effect of the ionosphere under quiet, nominal conditions. Ionospheric models can be generally divided into the following groups: theoretical models, empirical models, Global Navigation Satellite System (GNSS) data driven models and broadcast models (Orús et al., 2002). The theoretical models, such as coupled thermosphere–ionosphere model (CTIM) (Fuller-Rowell & Rees, 1980), thermosphere–ionosphere–electrodynamic general circulation model (TIEGCM) (Richmond et al., 1992), thermosphere ionosphere nested grid (TING) (W. Wang et al., 1999), and global ionosphere thermosphere model (GITM) (Ridley et al., 2006), could provide the physical theoretical prediction of ionospheric environment. The empirical models, such as IRI (Bilitza, 2001; Bilitza et al., 1990) and Nequick model (Di Giovanni & Radicella, 1990; Nava et al., 2008) , could define the empirical ionospheric processes. The GNSS data driven models, such as the global ionospheric model (GIM) produced by ionospheric associated analysis centers Energy, Mines and Resources (EMR) (Gao et al., 1994), Jet Propulsion Laboratory (JPL) (Ho et al., 1996), Universitat Politècnica de Catalunya (UPC) (Juan et al., 1997), Center for Orbit Determination in Europe (CODE) (Schaer, 1999), European Space Agency (ESA) (Feltens, 2007) and Institute of Geodesy and Geophysics, Chinese Academy of Sciences (IGG, CAS) (Li et al., 2015), could provide the numerical prediction of ionospheric TECs. The broadcast model or navigation ionospheric model is the easiest way for the single frequency users to correct the ionospheric delay, owing to its balance between the computation form and model accuracy. Various navigation ionospheric models were developed for individual GNSS systems, such as GPS Klobuchar model (Klobuchar, 1987) and Galileo Nequick–G model (Bidaine & Warnant, 2011). GNSS systems routinely distribute the model coefficients with signals. The end users receive the coefficients and compute the corrections with specific algorithms.

The validation of navigation ionospheric models has been performed with the development of GNSS systems. The overall percentage reduction in rms error could be approximately 50% for GPS Klobuchar model. But the reduction was generally greater than 60% under adverse ionospheric conditions (Feess & Stephens, 1987). The Beidou Navigation Satellite System (BDS) navigation ionospheric model could contribute higher precision of correction in middle latitudes but relatively lower precision in lower latitudes. The positioning accuracy was improved by 7.8%∼35.3% comparing with Klobuchar model in northern hemisphere. But the accuracy was degraded dramatically in the southern hemisphere (Wu et al., 2013). Galileo Nequick–G model could mitigate the ionospheric delay by 72.4% in continents and 68.6% in global oceans (N. Wang et al., 2017). For single frequency positioning, the RMS of horizontal component was around 6 m and vertical component was about 10 m for 95% percentile (Perez et al., 2018).

Although the previous studies have focused on the validation of various navigation ionospheric models, few papers have studied the performance of BDS navigation ionospheric model during geomagnetic storms, especially during different types of storms. In this study, the effects of different classes of geomagnetic storms on the performance of the BDS navigation ionospheric model is investigated comprehensively. The differences in effects among distinctive storms are studied as well.

2 Data and Methodology

Geomagnetic storms could be classified based on the disturbance storm time (Dst) index (Loewe & Prölss, 1997). In this study, Dst data were extracted from combined files in the OMNIweb database (https://omniweb.gsfc.nasa.gov). Geomagnetic storms in solar cycle 24 were analyzed by classifying them into three types, namely Strong, Moderate and Weak. The threshold values applied in the classification are shown in Table 1 (see (Gonzalez et al., 1994)).

Table 1. Thresholds applied in the classification of geomagnetic storms

Type	Dst (nT)	ΔT(hours)
Strong	-100	3
Moderate	-50	2
Weak(typical substorm)	-30	1

Large number of geomagnetic storms have occurred during the chosen period. Moreover, different kinds of storms were intertwined in the time domain. Therefore, it is necessary to design a strategy to distinguish them. The basic strategy for the selection of storms is that the Dst should be as minimum as possible and the duration of each storm should be more than 12 hours. To identify the start epoch of the main phase, a reverse searching algorithm on the Dst time series was designed. The maximum duration for the searching was empirically set to 24 hours. The maximum Dst within this time span was searched and the epoch of this maximum Dst was identified as the start epoch. To ensure that each storm was independent and not influenced by another storm, a condition was applied that the Dst index for ten days before and after the main phase day must be greater than the minimum value for each individual class of storms. Eventually, five prominent cases were selected for each class of storms from 2015 to 2018. The main property of a geomagnetic storm is its main phase (Loewe & Prölss, 1997), which contributes largely to the observed effects (Astafyeva et al., 2014). The main phase, the related minimum Dst and duration of all storms taken into account in this study are shown in Table 2. MJD is the modified Julian date. The suffix 0 to each date refers to the start epoch while 1 represents the end epoch. Duration is the whole period of the main phase.

Table 2. The main phase of different types of storms from 2015 to 2018 (STR–Strong, MED–Moderate, MNM–Weak)

TYPE	MJD0	YEAR0	MON0	DAY0	DOY0	HOUR0	Dst0 (nT)	MJD1	YEAR1	MON1	DAY1	DOY1	HOUR1	Dst1 (nT)	Duration (hours)
	57098	2015	3	17	76	5	56	57098	2015	3	17	76	22	-223	17
	57195	2015	6	22	173	6	13	57196	2015	6	23	174	4	-204	22
STR	57302	2015	10	7	280	2	-9	57302	2015	10	7	280	22	-124	20
	57375	2015	12	19	353	22	43	57376	2015	12	20	354	22	-155	24
	58355	2018	8	25	237	8	19	58356	2018	8	26	238	6	-174	22
	57180	2015	6	7	158	19	24	57181	2015	6	8	159	8	-73	13
	57273	2015	9	8	251	20	-2	57274	2015	9	9	252	12	-98	16
MED	57406	2016	1	19	19	19	15	57407	2016	1	20	20	16	-93	21
	57838	2017	3	26	85	22	15	57839	2017	3	27	86	14	-74	16
	58064	2017	11	7	311	4	25	58065	2017	11	8	312	1	-74	21
	57544	2016	6	5	157	8	32	57545	2016	6	6	158	6	-44	22
	57716	2016	11	24	329	5	-12	57717	2016	11	25	330	5	-46	24
MNM	57784	2017	1	31	31	11	-5	57785	2017	2	1	32	9	-45	22
	57920	2017	6	16	167	7	30	57920	2017	6	16	167	23	-31	16
	58269	2018	5	31	151	21	5	58270	2018	6	1	152	19	-39	22

The basic form of the BDS navigation ionospheric model is similar to that of GPS. The only difference is the method to compute the amplitude and phase term of the model (Wu et al., 2013). The primary formula is illustrated as follows:

$$I_z^{'}(t) = \begin{cases} 5 \times 10^{-9} + A_2 cos[\frac{2\pi(t-50400)}{A_4}], & |t-50400| < A_4/4 \\ 5 \times 10^{-9} \qquad , & |t-50400| \geq A_4/4 \end{cases} \tag{1}$$

Wherein, $I_z^{'}(t)$ is the ionospheric vertical time delay on B1 band, t is the local time, A_2 is the amplitude term and A_4 is the period term, all in seconds. The amplitude and period term can be computed by 8 broadcasted coefficients given in the navigation files. Combined with a mapping function (Wu et al., 2013), the vertical time delay can be transferred to the signal path. Hence the slant delay could be derived from the vertical time delay and the speed of light.

The slant delay may be further converted to the slant total electron content (STEC) along the signal path with B1I frequency by:

$$STEC = D_{Ion} \times f_{B1I}^2 / 0.403 \tag{2}$$

Where $STEC$ is the slant TEC in TECu. D_{Ion} is the slant delay in meters. f_{B1I} is the B1I frequency in GHz.

In order to evaluate the performance of the BDS navigation ionospheric model during the main phase of different classes of storms, the real–measured STECs derived from GPS observations were used as reference. In order to achieve high precision STECs in each signal path, the data processing was performed as follows. The geometry–free combination of dual–frequency (L1/L2) GPS observations were utilized to compute the initial values of STECs for the ionospheric pierce points (IPPs). The phase smoothing code method was applied in this procedure. The instrumental biases including satellite and receiver differential codes biases (DCBs) were subtracted from the initial values accordingly. The DCBs were calculated by a post–processing method (see (Montenbruck et al., 2014)). Moreover, to reduce possible multipath and mapping function errors, the elevation mask angle was set to 20 degrees.

The observations were collected from 18 evenly distributed GPS stations in the Crustal Movement Observation Network of China (CMONOC). The sampling interval for the observations was 30 seconds. Figure 1 shows the distribution of those stations. The dotted line represents the geomagnetic equator, which was derived from the World Magnetic Model (WMM). The stations are located mostly in the middle and low geomagnetic latitudes. The GPS orbits were computed by the IGS SP3 precise ephemeris. The final Global Ionospheric model (GIM) from IGS was used to compute the instrumental biases. The coefficients of the navigation ionospheric model were extracted from IGS Navigation files (format in RINEX 2.x and RINEX 3.x).

The STECs computed by the navigation ionospheric model were compared with the corresponding real–measured STECs in the same path. The related statistics were performed for the main phase period in the latitude, local time and whole region domains, respectively. For the latitude domain, the range of differences involved in the statistics was set to 10∼50 degrees with a step of 2 degrees. The individual statistics were made for each latitudinal zone. For the local time domain, the whole day was set from 0∼24 LT with an interval of 2 hours. The statistics were calculated for each time interval. For the whole region domain, all differences were utilized in the statistics. The statistics were implemented for the China region.

The indices such as minimum (MIN), maximum (MAX), BIAS, root mean square error (RMSE) and relative error (REL) were applied in this study. The formulas are illustrated as follows.

$$\begin{aligned}
MIN &= minimum\{\Delta TEC_i\} \\
MAX &= maximum\{\Delta TEC_i\} \\
BIAS &= <\Delta TEC_i> \\
RMSE &= \sqrt{<\Delta TEC_i^2>} \\
REL &= RMSE/<TEC_{ref,i}> \times 100\% \\
\Delta TEC_i &= TEC_{ref,i} - TEC_{mdl,i}\,, i = 1, n
\end{aligned} \tag{3}$$

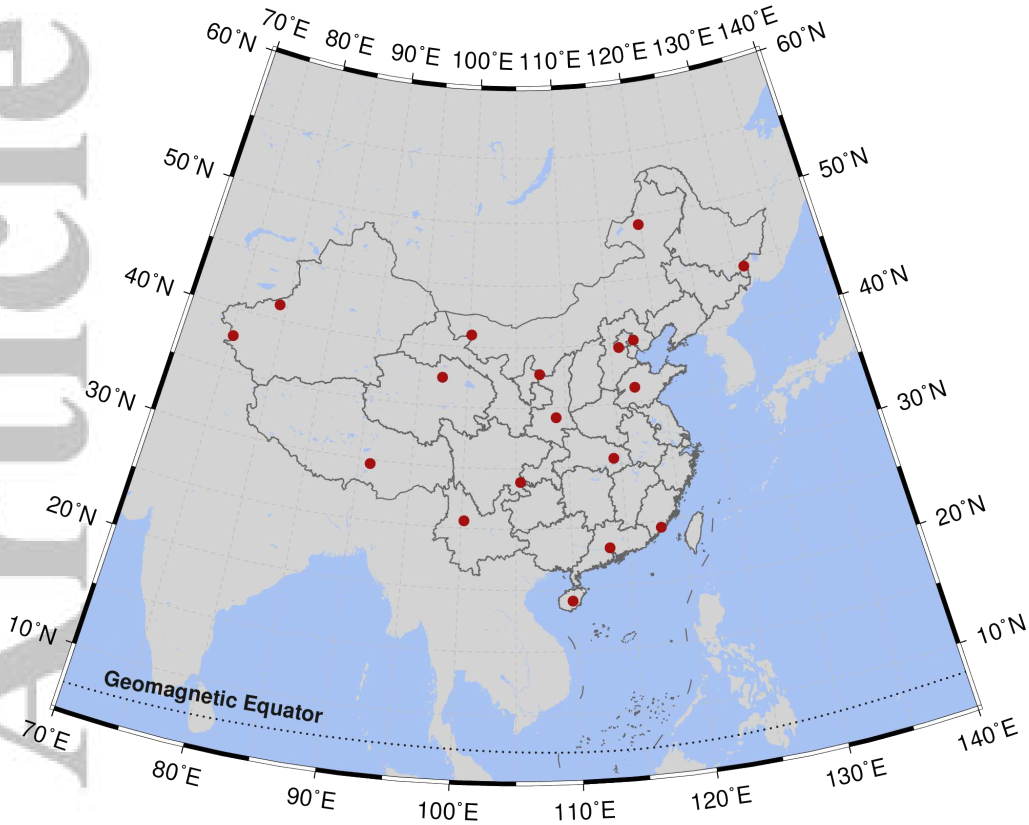

Figure 1. distribution of GPS stations from CMONOC network

Wherein, $<>$ is the average of the variable, $TEC_{ref,i}$ is the real–measured STEC, $TEC_{mdl,i}$ is the model STEC, n is the total number of samples.

3 Results and Discussions

Prior to presenting and discussing the results, the consistency analysis of GPS real–measured STECs with GIM derived STECs was performed. Figure 2 presents the histogram of the differences between GPS real–measured and GIM derived TECs during the main phase period of different classes of storms. MIN and MAX of the differences between real–measured TECs and GIM derived ones for different classes of storms are shown in the figure as well. As seen in the figure, the differences within 8 TECu accounted for more than 95% of the cases. In general, the data spread of differences for strong storms was the largest and the MAX was also largest. The scattering for moderate and weak storms seemed similar, while the MAX of moderate storms was larger than that of weak storms. The related statistical indices, namely BIAS and RMSE, are shown in Table 3. From the table, there are no obvious systematic offset between real–measured and GIM derived TECs for three storm classes. The BIAS for strong storms was the largest, while that for weak storms was the smallest. The RMSE for those three storms were 5.01 TECu, 3.74 TECu and 2.70 TECu respectively. Therefore, the real–measured TECs were quite consistent with the GIM derived ones. However, there were large discrepancies between them as shown in the MIN and MAX indices. It must be said that the observations for local region (especially China region) were not fully utilized in the ionospheric modeling in the IGS analysis centers (ACs). The mismodeling error for most of the ionospheric models in ACs was another factor. On the other hand, the large discrepancy could be the reflection of GIM accuracy during geomagnetic storms. Ionospheric activity might be more complicated during the storms, making it even harder for the ionospheric model to represent the real TECs.

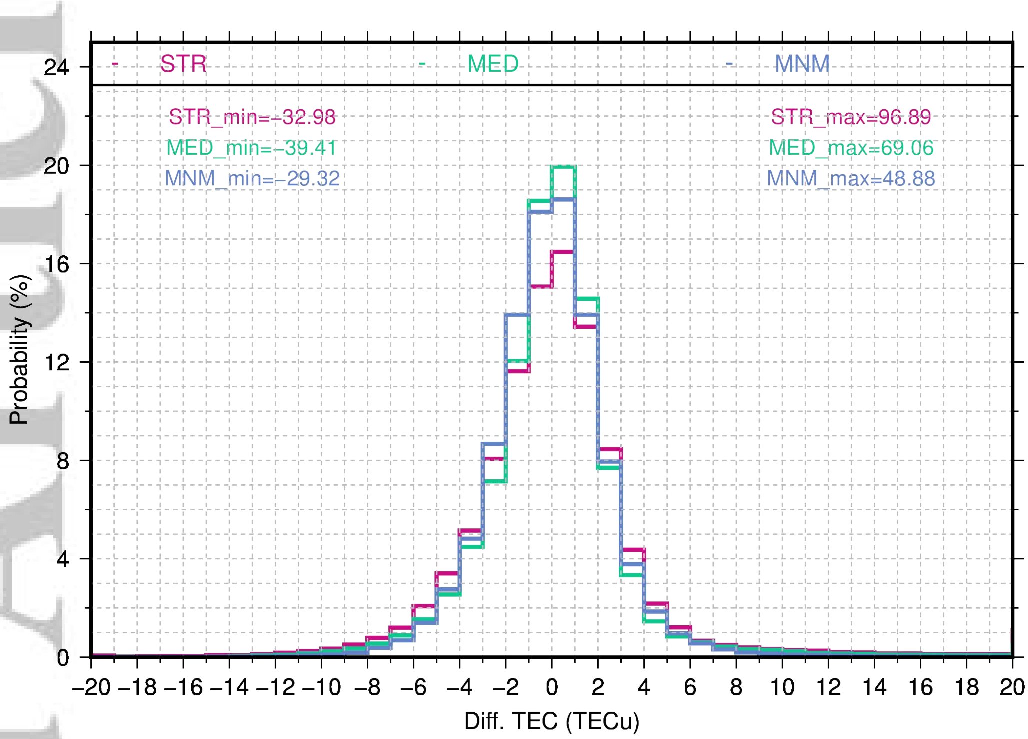

Figure 2. histogram of the differences between GPS real–measured TECs and GIM derived TECs (STR–Strong, MED–Moderate, MNM–Weak)

Table 3. BIAS and RMSE for the differences between real–measured TECs and GIM derived TECs during the main phase of geomagnetic storms (units: TECu)

Type	BIAS	RMSE
Strong	0.32	5.01
Moderate	0.18	3.74
Weak	-0.07	2.70

Figure 3 demonstrates the statistical indices for the BDS navigation ionospheric model during the main phase period in latitudinal domain. The legends represent different dates (in MJD) for different storm events. Each column indicates one type of storms. As shown in the figure, the indices clearly behave in accordance with the latitudinal characteristics during the main phase period. Especially, the indices variations in the low latitude were most intense. The largest changes for the indices occur near the geographical latitude 20 degrees (approximately at magnetic latitude of 15 degrees). The reason for that might be related to the equatorial ionospheric anomaly (EIA), a phenomenon characterized by the double peaked latitudinal distribution of electron density. The trough lies at the magnetic equator while the crest is at ±15∼20 dip latitude. In this region the ionospheric activity is the most complicated. During geomagnetic storms, the ionospheric activity could be enhanced or inhibited (Sreeja et al., 2009). Besides, the indices (BIAS, RMSE and REL) for the latitudes above 45 degrees are shown to be a little higher than those for the adjacent latitudes. That could be caused by the different negative or positive storm effect over mid–low latitudes for different cases. The negative ionospheric storm effects are primarily attributed to thermospheric composition changes (Fuller-Rowell et al., 1994). The mechanism of the positive storms remains complicated, which could be collectively triggered by the storm time equatorward thermospheric winds, prompt penetration electric fields (PPEF), disturbance dynamo electric fields (DDEF), traveling atmospheric disturbances (TADs), enhanced meridional wind, or a combination of them (Balan et al., 2010). This could be further studied in the next step. It is noticed that the indices for strong storm on MJD 57098 was the most distinctive. That suggests this storm event had a widespread influence on the China region. Specifically, the minimum of MIN was up to -42 TECu for strong storms, -40 TECu for moderate storms and -40 TECu for weak storms. The maximum of MAX was nearly 147 TECu for strong storms, 89 TECu for moderate storms and 44 TECu for weak storms. The range of BIAS was in -12∼28 TECu for strong storms, -21∼11 TECu for moderate storms and -14∼2 TECu for weak storms. The maximum of RMSE for strong storms was up to 38 TECu, while that was nearly 25 TECu for moderate storms and 16 TECu for weak storms. For REL, the maxima were 140%, 179% and 109% for strong, moderate and weak storms respectively. The mean and median of RMSE and REL for all latitude zones during each type of storm are illustrated in Table 4. The MEAN and MEDIAN of RMSE for strong storms were 11.19 and 7.48 TECu, while those for moderate storms were 7.78 and 6.72 TECu, and for weak storms were 6.34 and 5.85 TECu. The MEAN and MEDIAN of REL were 35.48% and 30.46% for strong storms, while those for moderate storms were 37.65% and 30.65% and for weak storms were 33.39% and 28.84%. Overall, the performance of the navigation ionospheric model during the main phase period of strong storms was the most unstable, followed by moderate and weak ones. In addition, the model accuracy was not comparable during the individual storms. That suggests the same class of storms may not have a consistent effect on the accuracy of navigation ionospheric model. The same feature could also be found in the other two aspects of the statistics (local time and the whole region domain).

Table 4. mean and median of RMSE and REL in latitudinal domain for all events of the individual type of storms

Type	RMSE (TECu)		REL (%)	
	MEAN	MEDIAN	MEAN	MEDIAN
Strong	11.19	7.48	35.48	30.46
Moderate	7.78	6.72	37.65	30.65
Weak	6.34	5.85	33.39	28.84

The statistics for the performance of the BDS navigation ionospheric model in the local time domain are demonstrated in Figure 4. Generally, the statistical indices were characterized to some extent by the diurnal changes. The changes in the indices were strongest around 14 LT. That suggests the accuracy of the model worsens when the ionospheric activity is more pronounced during the main phase of storms. From the individual indices in the figure, the minimum of MIN for strong storms was up to -42 TECu, whilst that was -47 TECu and -49 TECu for moderate and weak storms, respectively. The maxima of MAX were approximately 147, 89 and 44 TECu for strong, moderate and weak storms respectively. The range of BIAS for strong storms was -5∼34 TECu, while for moderate ones it was -7∼15 TECu and -12∼8 TECu for weak ones. The maximum of RMSE was up to 38 TECu for strong storms, 15 TECu for moderate ones and 12 TECu for weak ones. The maximum of REL was up to 83%, 110% and 119% for strong, mod-

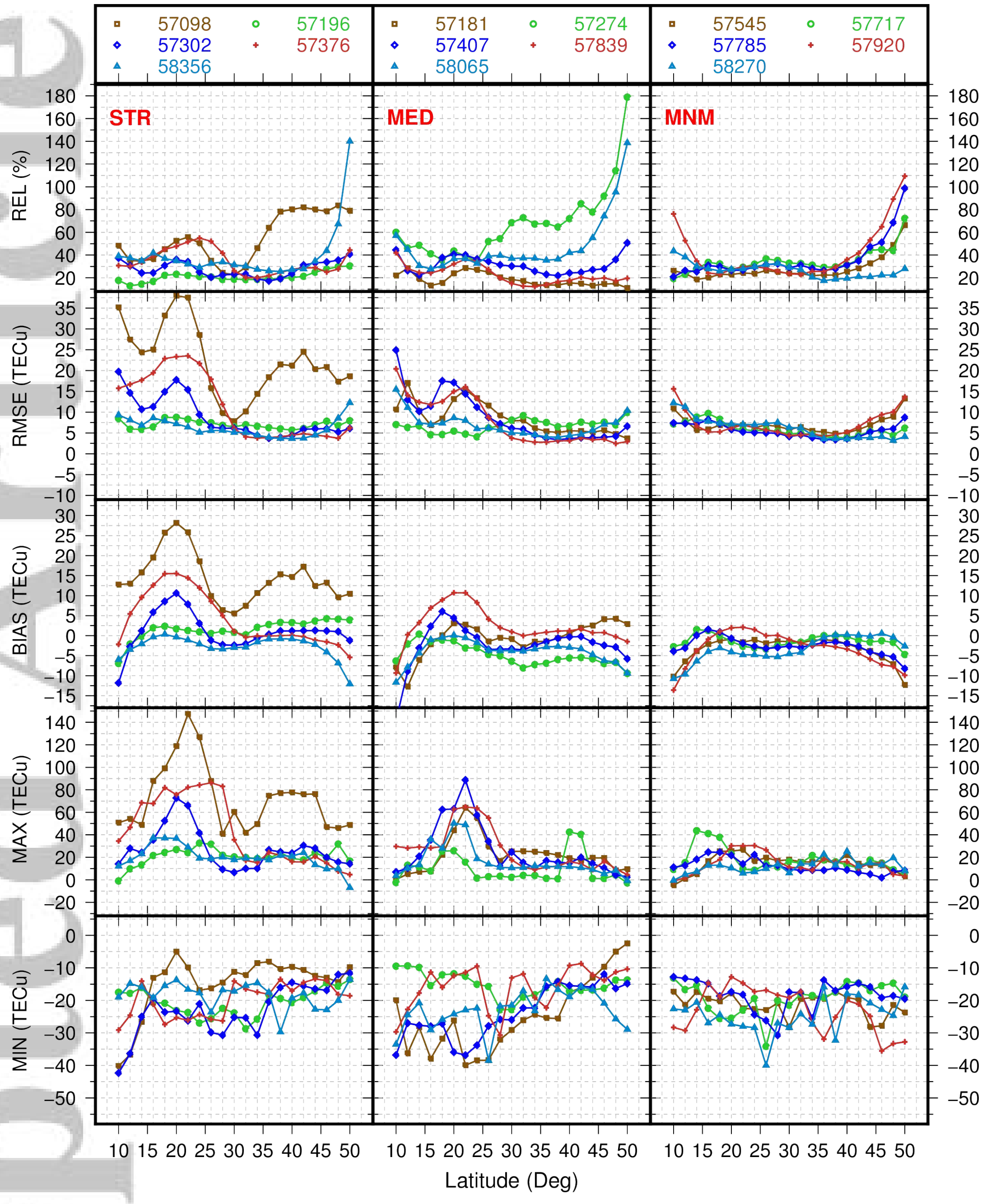

Figure 3. statistics for performance of BDS navigation ionospheric model with respect to latitude during main phase period (X–axis–geographic latitude, Y–axis–statistical indices; STR–Strong, MED–moderate, MNM–Weak)

erate and weak storms individually. The MEAN and MEDIAN of all RMSEs and RELs for different types of storms are shown in Table 5. The MEAN and MEDIAN of RMSE for strong storms were 9.33 and 6.33 TECu whilst those for moderate storms were 6.34 and 5.70 TECu and for weak storms were 5.37 and 5.12 TECu, respectively. For REL, the MEAN and MEDIAN were 34.03% and 30.87% for strong storms, 34.59% and 30.92% for moderate ones and 34.24% and 27.83% for weak ones. Therefore, the accuracy of the model suffered the largest influence during strong storms, followed by moderate and weak ones. It should be noticed that the indices, especially REL at nighttime, varied much more than those at adjacent epochs. This could be attributed to the nighttime constant assumption of the navigation ionospheric model (see constant offset term 5 ns in equation (1)). Ionospheric activity might become more complicated during geomagnetic storms, therefore it is not reasonable to set the nighttime term as constant over this period.

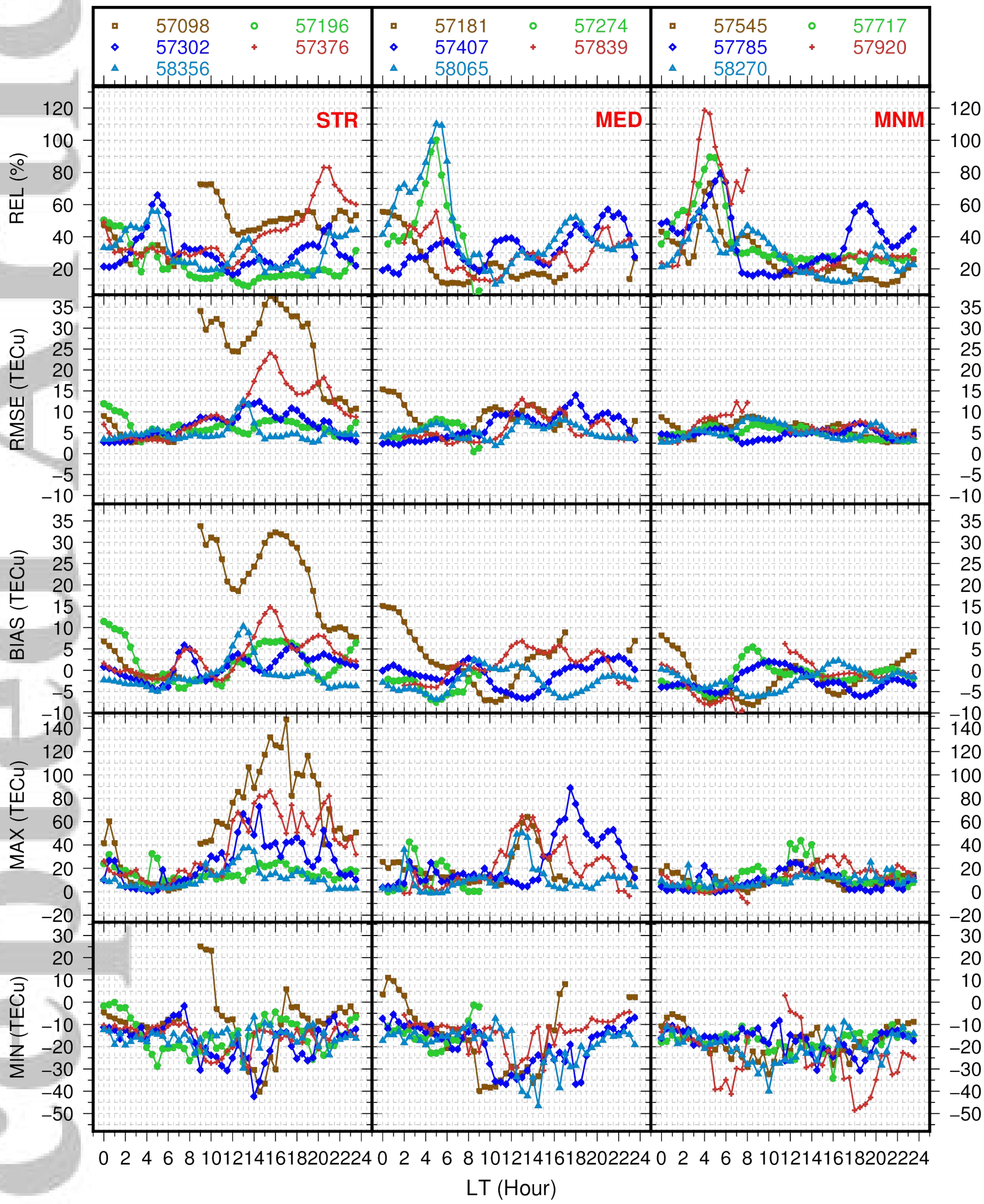

Figure 4. statistics for performance of BDS navigation ionospheric model with respect to local time during main phase period (X–axis–local time, Y–axis–statistical indices; STR–Strong, MED–Moderate, MNM–Weak)

Table 5. mean and median of RMSE and REL in local time domain for all events of the individual type of storms

Type	RMSE (TECu)		REL (%)	
	MEAN	MEDIAN	MEAN	MEDIAN
Strong	9.33	6.33	34.03	30.87
Moderate	6.34	5.70	34.59	30.92
Weak	5.37	5.12	34.24	27.83

The statistics were also performed for the whole China region in this study. The related results for different types of storms are illustrated in Tables 6∼8 separately. The first column names the date of storm event (in MJD). The last column means the number of samples involved in the statistics. The last two rows for each table are the mean and median of the related column. It can be concluded from the tables that most of the indices for strong storms were the largest, followed by moderate and weak ones. For strong storms, the minimum of MIN was -42.31 TECu, the maximum of MAX was 147.43 TECu, the BIAS was in the range of -1.69∼13.93 TECu, RMSE was up to 21.63 TECu and REL reached 57.73%. The MEAN and MEDIAN of RMSE were 10.58 and 7.56 TECu respectively. The comparison of indices between different events indicates that the influence was not consistent, even for the same class of storm. A similar phenomenon was also found in the statistics for moderate and weak storms. For moderate storms, the minimum of MIN was -46.54 TECu, the maximum of MAX was 88.77 TECu, the range of BIAS was in -5.33∼2.61 TECu, the maximum of RMSE was 8.45 TECu and that of REL was 63.68%. The MEAN and MEDIAN of RMSE were 7.19 and 7.17 TECu. The minimum of MIN for weak storms was -48.56 TECu and the maximum of MAX was 43.78 TECu. The BIAS was in range of -2.44∼1.29 TECu, respectively. The RMSE was up to 6.19 TECu and REL reached 34.48%. The MEAN and MEDIAN of RMSE were 5.52 and 5.49 TECu, respectively.

Table 6. the statistics for the whole region during the main phase of strong storms

MJD	MIN (TECu)	MAX (TECu)	BIAS (TECu)	RMSE (TECu)	REL (%)	NUM
57098	-40.19	147.43	13.93	21.63	57.73	205352
57196	-28.75	32.60	2.16	6.81	20.61	255947
57302	-42.31	72.76	1.11	7.56	28.95	227915
57376	-29.11	86.26	3.38	11.92	47.73	269263
58356	-29.71	37.52	-1.69	4.99	31.19	279771
MEAN	-34.01	75.31	3.78	10.58	37.24	
MEDIAN	-29.71	72.76	2.16	7.56	31.19	

4 Conclusions

In this study, the performance of the BDS navigation ionospheric model was analyzed comprehensively during the main phase of different classes of geomagnetic storms in the China region. From the statistical results, the performance of the model was affected to different degrees during the storms. Some conclusions can be reached specifically. Firstly, the influence on the accuracy of the model during strong storms is greatest, followed by moderate and weak storms. Secondly, the impact on the accuracy of the

Table 7. the statistics for the whole region during the main phase of moderate storms

MJD	MIN (TECu)	MAX (TECu)	BIAS (TECu)	RMSE (TECu)	REL (%)	NUM
57181	-39.92	64.08	0.05	8.45	19.78	147645
57274	-22.86	42.54	-5.33	6.96	63.68	43479
57407	-36.86	88.77	-1.27	7.63	36.04	256064
57839	-30.67	64.80	2.61	7.17	27.78	223889
58065	-46.54	50.25	-3.17	5.72	41.86	284510
MEAN	-35.37	62.09	-1.42	7.19	37.83	
MEDIAN	-36.86	64.08	-1.27	7.17	36.04	

Table 8. the statistics for the whole region during the main phase of weak storms

MJD	MIN (TECu)	MAX (TECu)	BIAS (TECu)	RMSE (TECu)	REL (%)	NUM
57545	-32.38	26.80	-2.00	6.19	25.79	259794
57717	-34.15	43.78	-1.29	5.08	33.72	330768
57785	-30.73	24.59	-2.44	4.72	32.91	303008
57920	-48.56	30.46	-2.16	6.14	34.48	215784
58270	-39.97	25.40	-2.23	5.49	25.86	291932
MEAN	-37.16	30.21	-2.02	5.52	30.55	
MEDIAN	-34.15	26.80	-2.16	5.49	32.91	

model is clearly characterized by the latitude and local time. Thirdly, the accuracy of the model is not always comparable even for the same class of storms, thus suggesting that the same class of storm does not have a consistent impact on the accuracy of the model.

This study could benefit the prediction of the navigation ionospheric model performance during geomagnetic storms. Especially, it could contribute to the improvement of the model in latitudinal and nighttime aspects during the storm time. Moreover, the impact of geomagnetic storms could be similar on other navigation systems such as GPS and Galileo. Thus these findings could provide a reference for future studies involving those systems. Nevertheless, the study period was in the downward phase of the solar cycle 24, when the solar activity was not strong, therefore the related effects on the accuracy of the navigation ionospheric model might not be quite noticeable. With the forthcoming solar cycle 25, the study could be performed more comprehensively.

Acknowledgments

The authors thank the anonymous referees for their valuable suggestions. Thanks to the IGS, MGEX and CMONOC for providing GNSS observations and products. The datasets analysed during the current study are available in the IGS MGEX repository [ftp://cddis.gsfc.nasa.gov/pub], NASA OMNI [https://omniweb.gsfc.nasa.gov] and CMONOC [http://data.earthquake.cn/datashare/report.shtml?PAGEID=siteInfo_jizhun]. This study is supported by National Natural Science Foundation of China (Grant No. 11703066) and a scholarship fund from the China Scholarship Council (CSC).The authors declare that they have no conflict of interest.

References

Amabayo, E. B., McKinnell, L.-A., & Cilliers, P. J. (2012). Ionospheric response over south africa to the geomagnetic storm of 11-13 april 2001 [Journal Article]. *Journal of Atmospheric and Solar-Terrestrial Physics*, *84-85*, 62-74. Retrieved from `http://www.sciencedirect.com/science/article/pii/S1364682612001459` doi: https://doi.org/10.1016/j.jastp.2012.06.002

Astafyeva, E., Yasyukevich, Y., Maksikov, A., & Zhivetiev, I. (2014). Geomagnetic storms, super-storms, and their impacts on gps-based navigation systems [Journal Article]. *Space Weather*, *12*(7), 508-525. Retrieved from `https://agupubs.onlinelibrary.wiley.com/doi/abs/10.1002/2014SW001072` doi: 10.1002/2014sw001072

Balan, N., Shiokawa, K., Otsuka, Y., Kikuchi, T., Vijaya Lekshmi, D., Kawamura, S., ... Bailey, G. J. (2010). A physical mechanism of positive ionospheric storms at low latitudes and midlatitudes [Journal Article]. *Journal of Geophysical Research: Space Physics*, *115*(A2). Retrieved from `https://agupubs.onlinelibrary.wiley.com/doi/abs/10.1029/2009JA014515` doi: 10.1029/2009ja014515

Bidaine, B., & Warnant, R. (2011). Ionosphere modelling for galileo single frequency users: Illustration of the combination of the nequick model and gnss data ingestion [Journal Article]. *Advances in Space Research*, *47*(2), 312-322. Retrieved from `http://www.sciencedirect.com/science/article/pii/S027311771000596X` doi: https://doi.org/10.1016/j.asr.2010.09.001

Bilitza, D. (2001). International reference ionosphere 2000 [Journal Article]. *Radio Science*, *36*(2), 261-275.

Bilitza, D., Rawer, K., Bossy, L., Kutiev, I., Oyama, K.-I., Leitinger, R., & Kazimirovsky, E. (1990). International reference ionosphere 1990 [Journal Article].

Blagoveshchenskii, D. V. (2013). Effect of geomagnetic storms (substorms) on the ionosphere: 1. a review [Journal Article]. *Geomagnetism and Aeronomy*, *53*(3), 275-290. doi: 10.1134/s0016793213030031

Chakraborty, M., Kumar, S., De, B. K., & Guha, A. (2015). Effects of geomagnetic storm on low latitude ionospheric total electron content: A case study from indian sector [Journal Article]. *Journal of Earth System Science*, *124*(5), 1115-1126. Retrieved from `https://doi.org/10.1007/s12040-015-0588-3` doi: 10.1007/s12040-015-0588-3

D'Angelo, G., Piersanti, M., Alfonsi, L., Spogli, L., Clausen, L. B. N., Coco, I., ... Baiqi, N. (2018). The response of high latitude ionosphere to the 2015 st. patricks day storm from in situ and ground based observations [Journal Article]. *Advances in Space Research*, *62*(3), 638-650. Retrieved from `http://www.sciencedirect.com/science/article/pii/S0273117718304010` doi: https://doi.org/10.1016/j.asr.2018.05.005

Danilov, A., & Lastovicka, J. (2001). Effects of geomagnetic storms on the ionosphere and atmosphere [Journal Article]. *International Journal of Geomagnetism and Aeronomy*, *2*(3), 209-224.

Di Giovanni, G., & Radicella, S. M. (1990). An analytical model of the electron density profile in the ionosphere [Journal Article]. *Advances in Space Research*, *10*(11), 27-30. Retrieved from `http://www.sciencedirect.com/science/article/pii/027311779090301F` doi: https://doi.org/10.1016/0273-1177(90)90301-F

Dujanga, F. M., Baki, P., Olwendo, J. O., & Twinamasiko, B. F. (2013). Total electron content of the ionosphere at two stations in east africa during the 24c25 october 2011 geomagnetic storm [Journal Article]. *Advances in Space Research*, *51*(5), 712-721. Retrieved from `http://www.sciencedirect.com/science/article/pii/S0273117712006308` doi: https://doi.org/10.1016/j.asr.2012.09.040

Echer, E., Gonzalez, W. D., Tsurutani, B. T., & Gonzalez, A. L. C. (2008).

Interplanetary conditions causing intense geomagnetic storms (dst 100 nt) during solar cycle 23 (1996c2006) [Journal Article]. *Journal of Geophysical Research: Space Physics*, *113*(A5). Retrieved from `https://agupubs.onlinelibrary.wiley.com/doi/abs/10.1029/2007JA012744` doi: 10.1029/2007ja012744

Feess, W., & Stephens, S. (1987). Evaluation of gps ionospheric time-delay model [Journal Article]. *Aerospace and Electronic Systems, IEEE Transactions on*(3), 332-338.

Feltens, J. (2007). Development of a new three-dimensional mathematical ionosphere model at european space agency/european space operations centre [Journal Article]. *Space Weather*, *5*(12).

Fuller-Rowell, T. J., Codrescu, M. V., Moffett, R. J., & Quegan, S. (1994). Response of the thermosphere and ionosphere to geomagnetic storms [Journal Article]. *Journal of Geophysical Research: Space Physics*, *99*(A3), 3893-3914. Retrieved from `https://agupubs.onlinelibrary.wiley.com/doi/abs/10.1029/93JA02015` doi: 10.1029/93ja02015

Fuller-Rowell, T. J., & Rees, D. (1980). A three-dimensional time-dependent global model of the thermosphere [Journal Article]. *Journal of the Atmospheric Sciences*, *37*(11), 2545-2567. Retrieved from `https://journals.ametsoc.org/doi/abs/10.1175/1520-0469%281980%29037%3C2545%3AATDTDG%3E2.0.CO%3B2` doi: 10.1175/1520-0469(1980)037⟨2545:Atdtdg⟩2.0.Co;2

Gao, Y., Heroux, P., & Kouba, J. (1994). Estimation of gps receiver and satellite l1/l2 signal delay biases using data from cacs [Conference Proceedings]. In *International symposium on kinematic systems in geodesy, geomatics and navigation* (p. 8).

Gonzalez, W. D., Joselyn, J. A., Kamide, Y., Kroehl, H. W., Rostoker, G., Tsurutani, B. T., & Vasyliunas, V. M. (1994). What is a geomagnetic storm? [Journal Article]. *Journal of Geophysical Research: Space Physics*, *99*(A4), 5771-5792. Retrieved from `https://agupubs.onlinelibrary.wiley.com/doi/abs/10.1029/93JA02867` doi: 10.1029/93ja02867

Gonzalez, W. D., Tsurutani, B. T., & De Gonzalez, A. L. C. (1999). Interplanetary origin of geomagnetic storms [Journal Article]. *Space Science Reviews*, *88*(3-4), 529-562.

Heelis, R. A., Sojka, J. J., David, M., & Schunk, R. W. (2009). Storm time density enhancements in the middle-latitude dayside ionosphere [Journal Article]. *Journal of Geophysical Research: Space Physics*, *114*(A3). Retrieved from `https://agupubs.onlinelibrary.wiley.com/doi/abs/10.1029/2008JA013690` doi: 10.1029/2008ja013690

Ho, C. M., Mannucci, A. J., Lindqwister, U. J., Pi, X., & Tsurutani, B. T. (1996). Global ionosphere perturbations monitored by the worldwide gps network [Journal Article]. *Geophysical Research Letters*, *23*(22), 3219-3222. Retrieved from `https://agupubs.onlinelibrary.wiley.com/doi/abs/10.1029/96GL02763` doi: 10.1029/96gl02763

Juan, J. M., Rius, A., Hernández-Pajares, M., & Sanz, J. (1997). A two-layer model of the ionosphere using global positioning system data [Journal Article]. *Geophysical Research Letters*, *24*(4), 393-396.

Klobuchar, J. A. (1987). Ionospheric time-delay algorithm for single-frequency gps users [Journal Article]. *Aerospace and Electronic Systems, IEEE Transactions on*(3), 325-331.

Lastovicka, J. (1996). Effects of geomagnetic storms in the lower ionosphere, middle atmosphere and troposphere [Journal Article]. *Journal of Atmospheric and Terrestrial Physics*, *58*(7), 831-843. Retrieved from `<GotoISI>://WOS:A1996UC38200002` doi: Doi10.1016/0021-9169(95)00106-9

Li, Z., Yuan, Y., Wang, N., Hernandez-Pajares, M., & Huo, X. (2015). Shpts: towards a new method for generating precise global ionospheric tec map based on spherical harmonic and generalized trigonometric series functions [Journal Article]. *Journal of Geodesy*, *89*(4), 331-345. Retrieved from `https://doi.org/10.1007/s00190-014-0778-9` doi: 10.1007/s00190-014-0778-9

Loewe, C. A., & Prölss, G. W. (1997). Classification and mean behavior of magnetic storms [Journal Article]. *Journal of Geophysical Research: Space Physics*, *102*(A7), 14209-14213. doi: 10.1029/96ja04020

Montenbruck, O., Hauschild, A., & Steigenberger, P. (2014). Differential code bias estimation using multi-gnss observations and global ionosphere maps [Journal Article]. *Navigation*, *61*(3), 191-201.

Nava, B., Coïsson, P., & Radicella, S. M. (2008). A new version of the nequick ionosphere electron density model [Journal Article]. *Journal of Atmospheric and Solar-Terrestrial Physics*, *70*(15), 1856-1862. Retrieved from `http://www.sciencedirect.com/science/article/pii/S1364682608000357` doi: https://doi.org/10.1016/j.jastp.2008.01.015

Ngwira, C. M., McKinnell, L.-A., Cilliers, P. J., & Yizengaw, E. (2012). An investigation of ionospheric disturbances over south africa during the magnetic storm on 15 may 2005 [Journal Article]. *Advances in Space Research*, *49*(2), 327-335. Retrieved from `http://www.sciencedirect.com/science/article/pii/S0273117711007174` doi: https://doi.org/10.1016/j.asr.2011.09.035

Orús, R., Hernández-Pajares, M., Juan, J., Sanz, J., & García-Fernández, M. (2002). Performance of different tec models to provide gps ionospheric corrections [Journal Article]. *Journal of Atmospheric and Solar-Terrestrial Physics*, *64*(18), 2055-2062.

Perez, R. O., Parro-Jimenez, J. M., & Prieto-Cerdeira, R. (2018). Status of nequick g after the solar maximum of cycle 24 [Journal Article]. *Radio Science*, *53*(3), 257-268. Retrieved from `<GotoISI>://WOS:000430185100002` doi: 10.1002/2017rs006373

Richmond, A. D., Ridley, E. C., & Roble, R. G. (1992). A thermosphere/ionosphere general circulation model with coupled electrodynamics [Journal Article]. *Geophysical Research Letters*, *19*(6), 601-604. Retrieved from `https://agupubs.onlinelibrary.wiley.com/doi/abs/10.1029/92GL00401` doi: 10.1029/92gl00401

Ridley, A. J., Deng, Y., & Tth, G. (2006). The global ionospherecthermosphere model [Journal Article]. *Journal of Atmospheric and Solar-Terrestrial Physics*, *68*(8), 839-864. Retrieved from `http://www.sciencedirect.com/science/article/pii/S1364682606000071` doi: https://doi.org/10.1016/j.jastp.2006.01.008

Schaer, S. (1999). Mapping and predicting the earth's ionosphere using the global positioning system [Journal Article]. *Geod.-Geophys. Arb. Schweiz*, *59*.

Sreeja, V., Devasia, C. V., Ravindran, S., Pant, T. K., & Sridharan, R. (2009). Response of the equatorial and low-latitude ionosphere in the indian sector to the geomagnetic storms of january 2005 [Journal Article]. *Journal of Geophysical Research: Space Physics*, *114*(A6). Retrieved from `https://agupubs.onlinelibrary.wiley.com/doi/abs/10.1029/2009JA014179` doi: 10.1029/2009ja014179

Wang, N., Yuan, Y., Li, Z., Li, Y., Huo, X., & Li, M. (2017). An examination of the galileo nequick model: comparison with gps and jason tec [Journal Article]. *GPS Solutions*, *21*(2), 605-615. Retrieved from `https://doi.org/10.1007/s10291-016-0553-x` doi: 10.1007/s10291-016-0553-x

Wang, W., Killeen, T. L., Burns, A. G., & Roble, R. G. (1999). A high-resolution, three-dimensional, time dependent, nested grid model of the coupled thermospherecionosphere [Journal Article]. *Journal of Atmospheric and Solar-Terrestrial Physics*, *61*(5), 385-397. Retrieved from `http://www.sciencedirect.com/science/article/pii/S1364682698000790` doi: https://doi.org/10.1016/S1364-6826(98)00079-0

Wu, X., Hu, X., Wang, G., Zhong, H., & Tang, C. (2013). Evaluation of compass ionospheric model in gnss positioning [Journal Article]. *Advances in Space Research*, *51*(6), 959-968. Retrieved from http://www.sciencedirect.com/science/article/pii/S0273117712006291 doi: https://doi.org/10.1016/j.asr.2012.09.039

Figure 1.

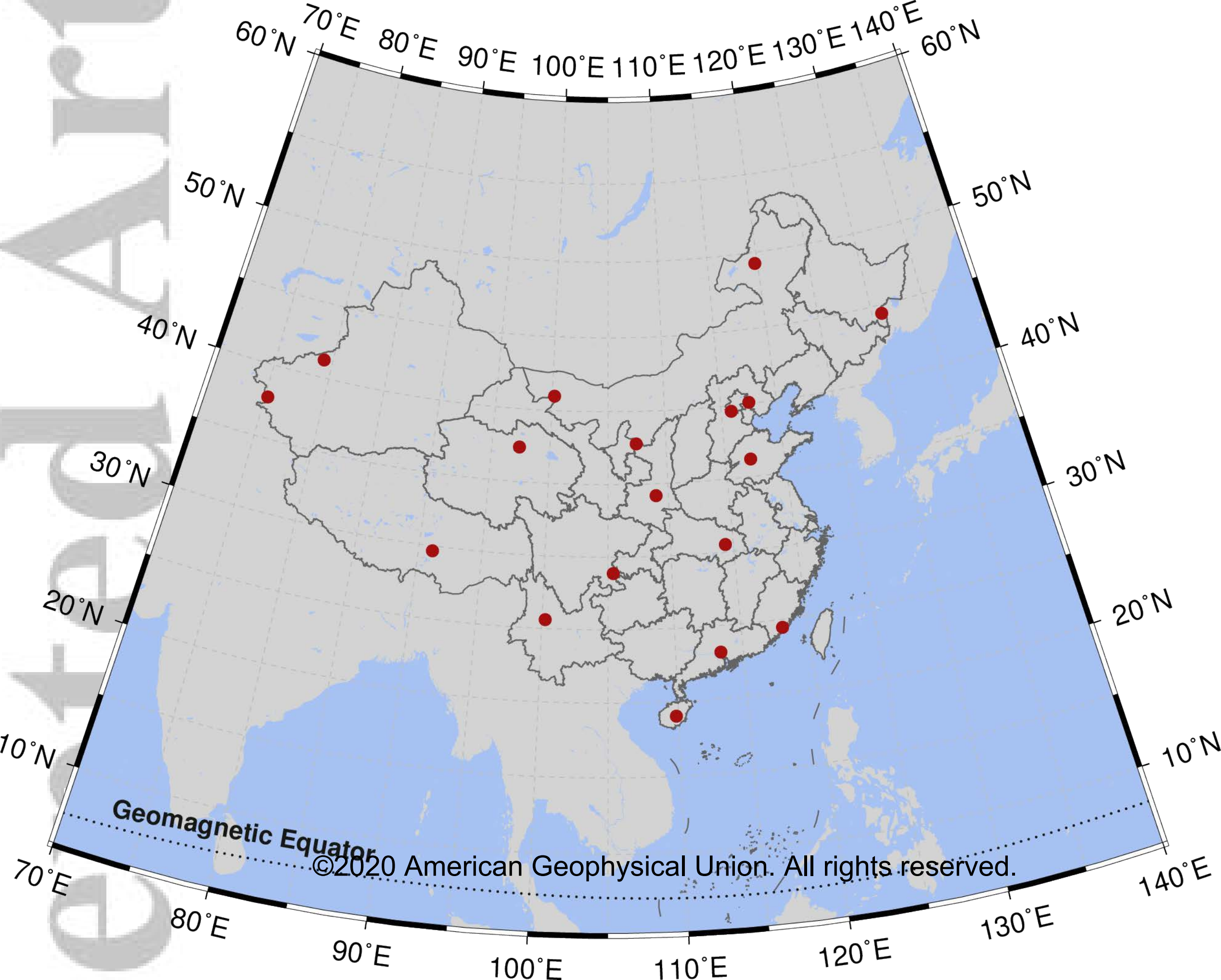
70°E
80°E
90°E
100°E
110°E
120°E
130°E
140°E
60°N
50°N
40°N
30°N
20°N
10°N
Geomagnetic Equator

Figure 2.

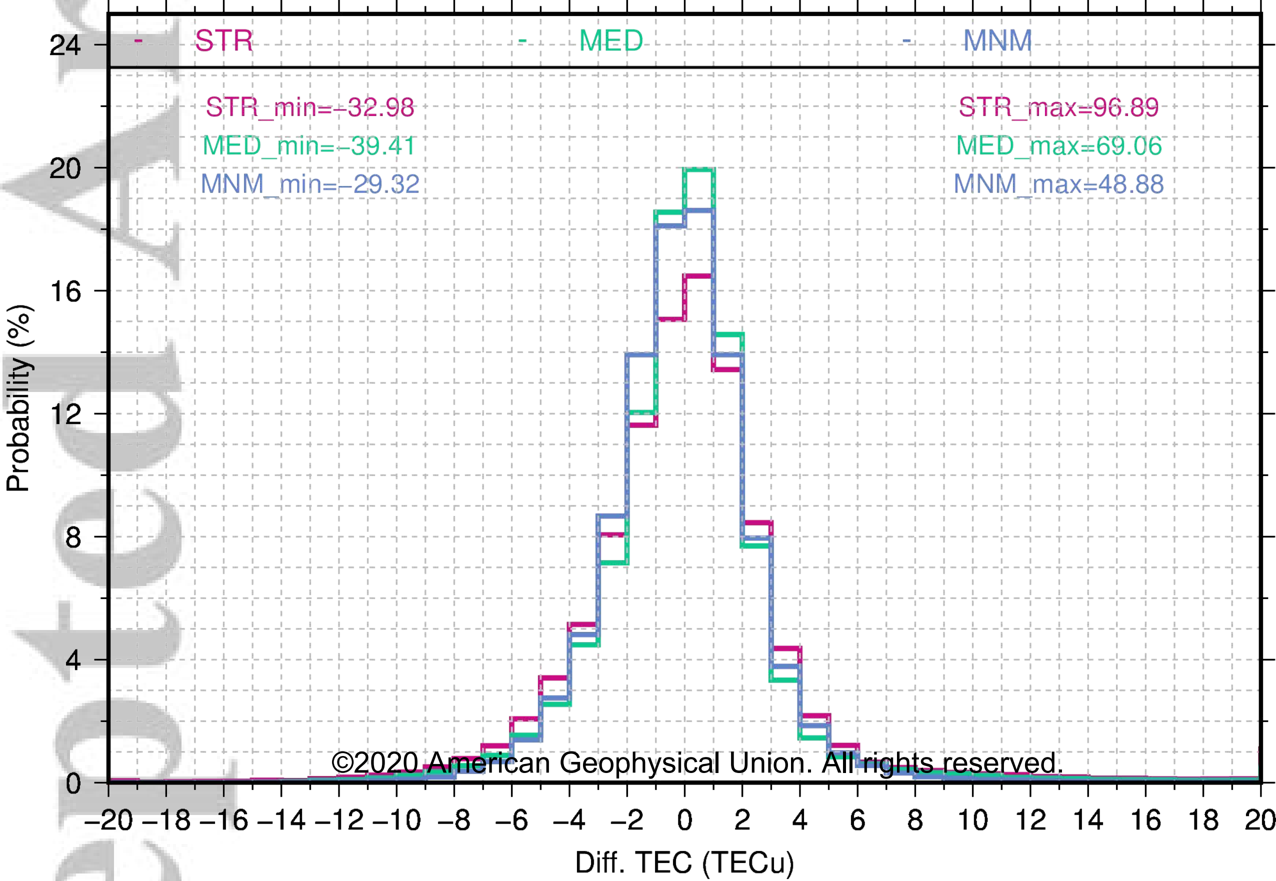

STR
MED
MNM
STR_min=−32.98
MED_min=−39.41
MNM_min=−29.32
STR_max=96.89
MED_max=69.06
MNM_max=48.88
Probability (%)
Diff. TEC (TECu)

Figure 3.

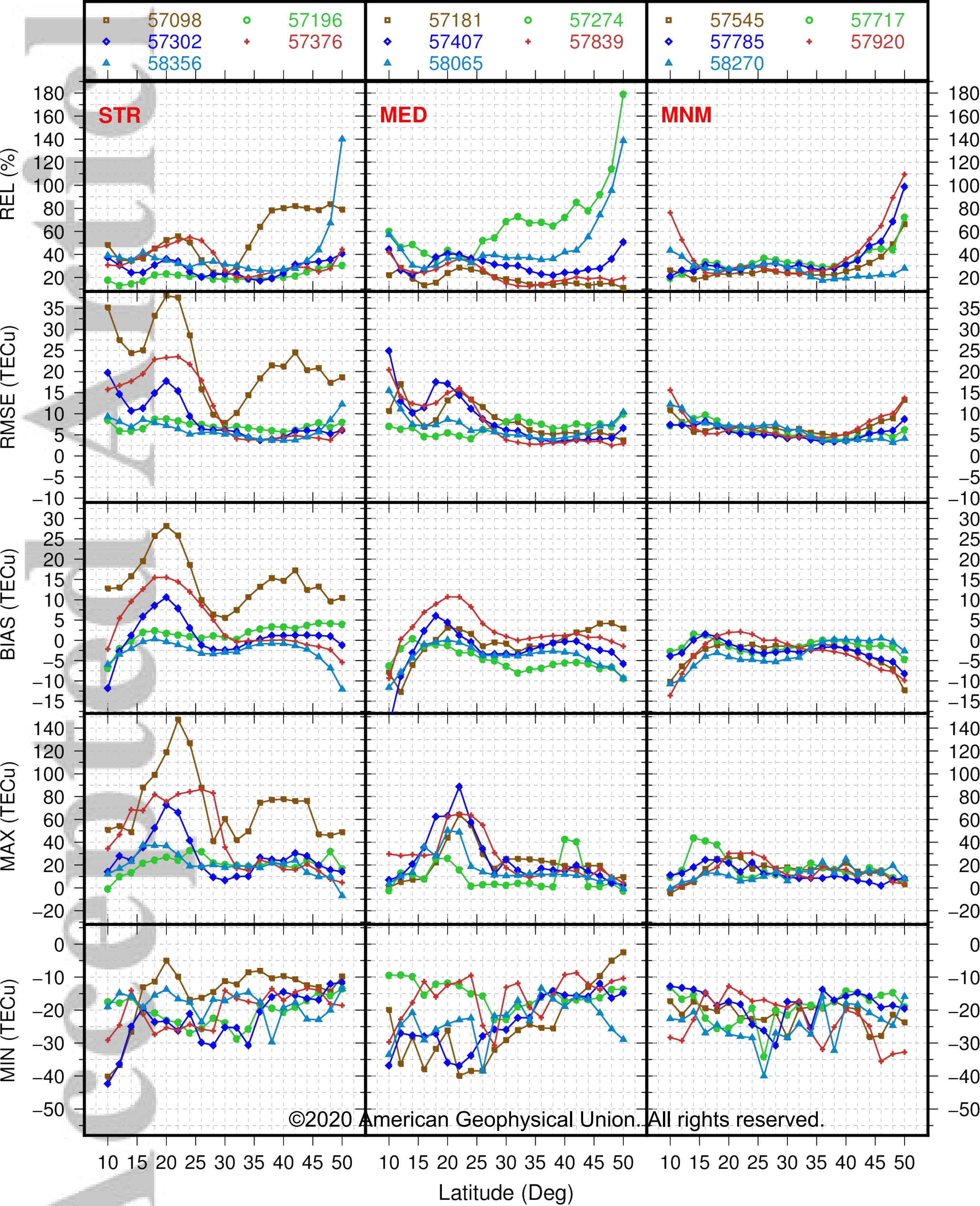
57098
57196
57302
57376
58356
57181
57274
57407
57839
58065
57545
57717
57785
57920
58270
STR
MED
MNM
REL (%)
RMSE (TECu)
BIAS (TECu)
MAX (TECu)
MIN (TECu)
Latitude (Deg)

Figure 4.

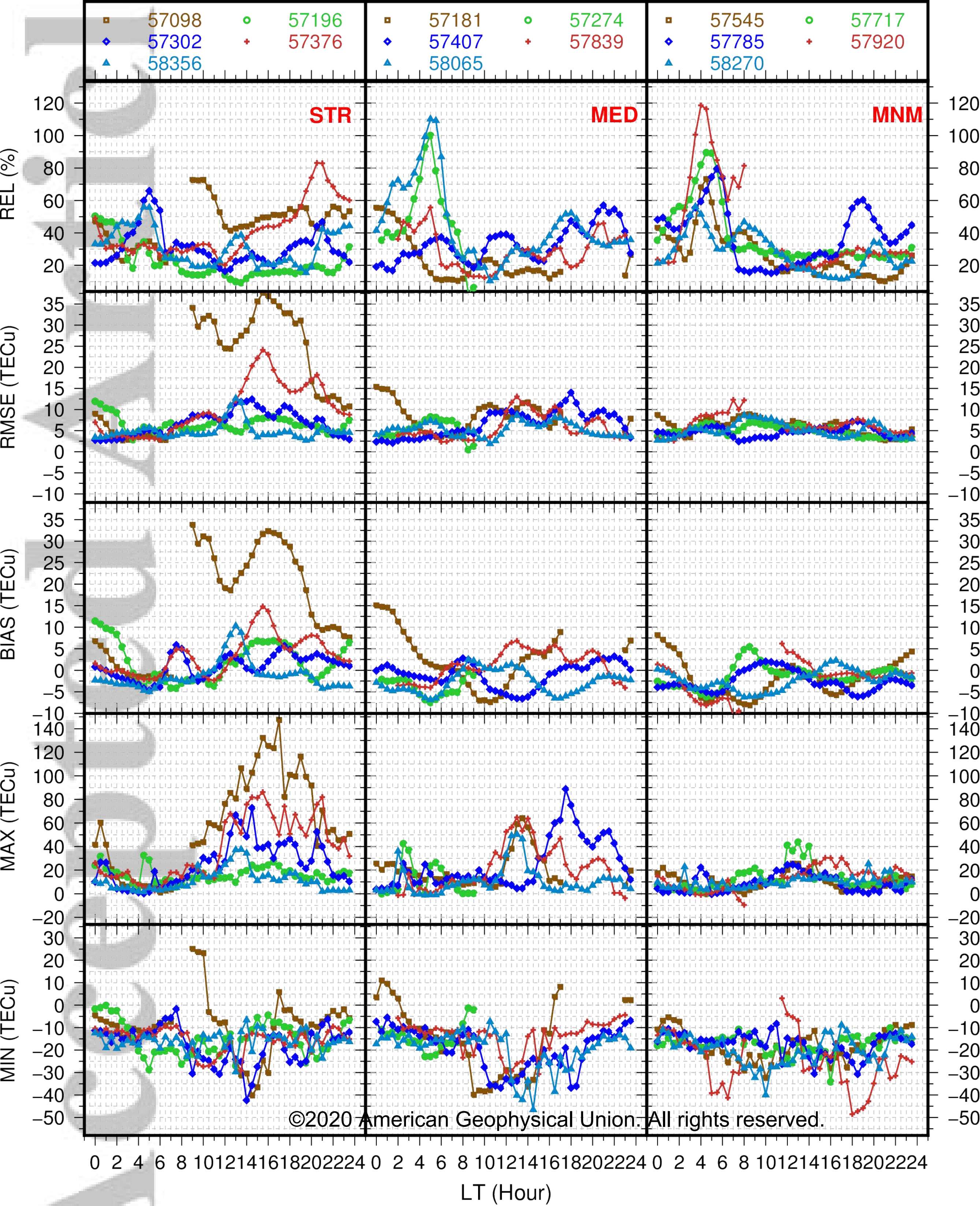
57098
57196
57302
57376
58356
57181
57274
57407
57839
58065
57545
57717
57785
57920
58270
STR
MED
MNM
REL (%)
RMSE (TECu)
BIAS (TECu)
MAX (TECu)
MIN (TECu)
LT (Hour)